POLITECNICO DI TORINO
Repository ISTITUZIONALE

Gas drainage interception technology for roadway between coal seams passing through geological abnormal areas

Original
Gas drainage interception technology for roadway between coal seams passing through geological abnormal areas / Ren, F., Wang, C., Li, J., Su, W.. - In: GEOMECHANICS AND GEOENGINEERING. - ISSN 1748-6025. - (2025), pp. 1-20. [10.1080/17486025.2025.2456554]

Availability:
This version is available at: 11583/2997286 since: 2025-02-06T17:54:08Z

Publisher:
Taylor & Francis

Published
DOI:10.1080/17486025.2025.2456554

Terms of use:

This article is made available under terms and conditions as specified in the corresponding bibliographic description in the repository

Publisher copyright
Springer postprint/Author's Accepted Manuscript

This version of the article has been accepted for publication, after peer review (when applicable) and is subject to Springer Nature's AM terms of use, but is not the Version of Record and does not reflect post-acceptance improvements, or any corrections. The Version of Record is available online at: http://dx.doi.org/10.1080/17486025.2025.2456554

(Article begins on next page)

28 November 2026

Gas drainage interception technology for roadway between coal seams passing through geological abnormal areas

Fake Ren [1,2], Chongyang Wang [1,2,3*], Jie Li [1,2,4,5], Weiwei Su [4,5]

1. State Key Laboratory of Coal Mine Disaster Dynamics and Control, Chongqing University, Chongqing 400044, China,

2. School of Resources and Safety Engineering, Chongqing University, Chongqing 400044, China,

3. Department of Structural, Geotechnical and Building Engineering, Politecnico di Torino, Turin, Italy.

4. China Coal Technology and Engineering Group Shenyang Research Institute, Fushun 113122, China;

5. State Key Laboratory of Coal Mine Safety Technology, Fushun 113122, China.

**Corresponding author: Chongyang Wang, 20212001033@cqu.edu.cn (wcy@cqu.edu.cn).*

Abstract: To address the issue of gas accumulation in the working face when roadways between coal seams pass through geologically abnormal areas, based on the summary and classification of existing gas drainage methods, gas drainage interception technology was proposed, and its technical concept, principle, and application process were elaborated. The 221 East Wing Track Roadway of the Liu Jia Liang Coal Mine was selected as the test site. Following the gas drainage interception process, the gas flow path, primary gas source, and the loose zone of the surrounding roadway rock were systematically examined. Results indicated that the gas flow path of the working face is predominantly located in its upper front; the primary gas source is the 5# coal seam beneath the roadway; and the loose zone of the surrounding rock ranges from 0.65 to 2.30 meters. Consequently, a dual high- negative-pressure and low-negative-pressure drainage interception technology was implemented to capture gas within the fractures around the roadway. Trial excavations confirmed that this method effectively intercepted gas within the rock fractures, ensuring safe excavation operations.

Keywords: Roadway between coal seams; Geological abnormal areas; Gas drainage methods; Gas

drainage interception technology.

1. Introduction

Due to varying geological conditions across different areas of the mine field, some roadways inevitably traverse unfavorable geological sections, such as fault fracture zones, densely jointed areas, and weak interlayers during tunneling. Taking the fault fracture zone as an example, the rock mass near these zones exhibits distinct differences in physical and mechanical properties due to characteristics such as low strength, susceptibility to deformation, high permeability, and poor water resistance [1-3]. Particularly, when a roadway is situated near a coal seam and connected to it through rock fractures, gas from the coal seam may migrate into the roadway's working space, driven by its pressure gradient. Therefore, alongside adopting appropriate excavation and support techniques, the selection of effective gas control technology is crucial.

When excavating roadways between coal seams in geologically abnormal areas, gas emission and accumulation are inevitable if the roadway connects to a high-gas-content coal seam through rock fractures. This presents significant safety challenges during excavation. Numerous scholars have extensively researched various aspects of this issue. Regarding gas seepage characteristics, studies increasingly demonstrate that Darcy’s law applies only to laminar flow with low Reynolds numbers (Re), while other seepage conditions must be described using non-Darcy flow models [4-5]. For the porous medium of coal and rock, internal gas seepage is influenced by intrinsic factors such as bedding (joint) distribution, porosity, particle size, and connectivity, as well as external factors like stress state and vibration frequency [6-10]. In terms of gas drainage technology, coal mine methane (CMM) drainage can be categorized into underground CMM drainage, surface CMM drainage, and combined surface and underground CMM drainage. Underground drainage methods primarily include in-seam (cross) borehole drainage, cross-

measure borehole drainage, coal seam roadway drainage, horizontal long borehole drainage, gob buried pipe drainage, and drainage from high-level roadways or boreholes within the gob. Surface CMM drainage techniques include gob surface drainage, stress-relieved seam surface well drainage, multi-branch horizontal directional well drainage, and multipurpose surface well drainage, among others [11]. Additionally, for low-permeability coal seams, technologies such as hydraulic fracturing, hydraulic flushing, hydraulic slotting, large-diameter mechanical cave-making, coal seam gas injection, CO_2 phase transition jet coal breaking, and other permeability enhancement techniques have been developed and applied to improve gas drainage efficiency [12-17].

Significant advancements have been made in the study of gas seepage characteristics and gas drainage technologies. However, there remains a lack of research on gas control technologies for roadways located between coal seams in geologically abnormal areas, particularly where the distribution of rock fractures is uncertain. The selection of appropriate gas control techniques and ensuring safe roadway construction under these conditions require further investigation. In response to this need, this paper focusing on the gas control challenges encountered when roadways pass through geologically abnormal areas, this study proposes the gas drainage interception technology, detailing its principles, connotation, and application process. Using the case study of gas emission and accumulation during the excavation of the 221 East Wing Track Roadway at Liu Jia Liang Coal Mine, the paper applies this technology by identifying gas flow channels, determining the main gas source, and delineating the loose zone of surrounding rock. High and low negative pressure dual gas drainage interception boreholes were then arranged around the roadway to capture gas from fractures in the surrounding rock. The effectiveness of this approach was verified through trial excavation.

2. Characteristics of gas drainage interception technology

2.1 Technology connotation

Gas drainage is a fundamental technical measure employed to mitigate gas disasters in coal mines. Based on the temporal relationship between gas drainage and mining operations, it can be classified into three categories: pre-drainage, drainage during mining, and post-drainage [18]. Additionally, according to the primary function of each drainage method [19-22], these methods can be further divided into two categories: those aimed at reducing the gas content of the gas source and those focused on altering the gas flow path, as illustrated in Fig. 1.

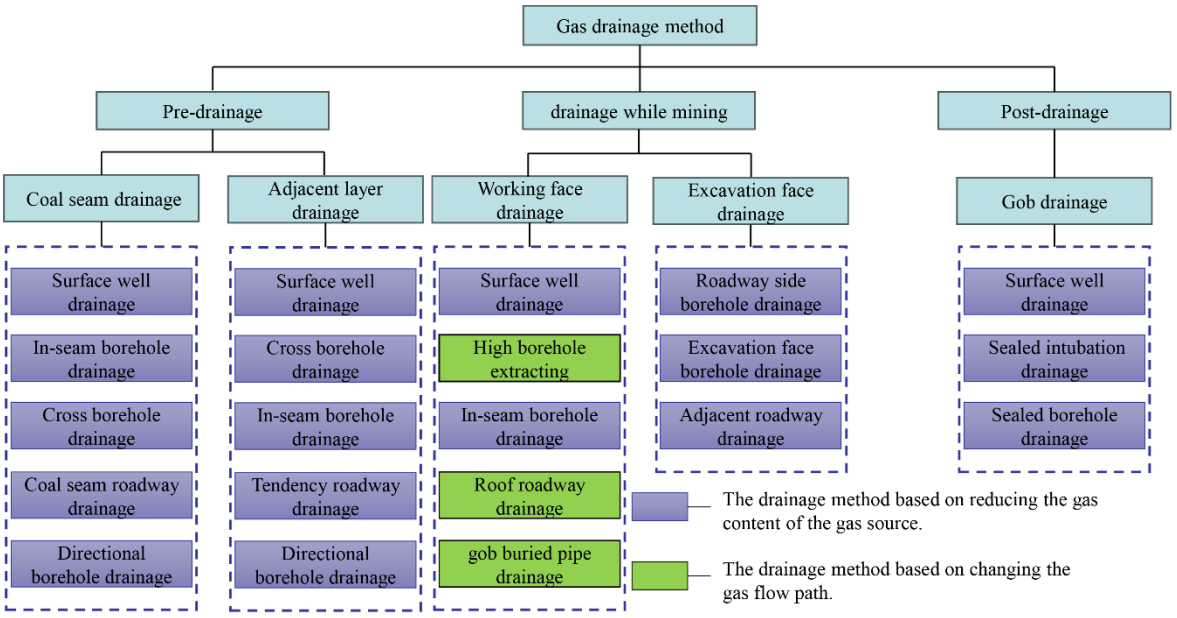


Fig. 1 Classification of gas drainage methods

The drainage method designed to reduce the gas content of the gas source primarily involves the construction of drainage boreholes or wells that connect to the gas source (i.e., coal seam or gas accumulation area). This method effectively diminishes the gas content, thereby reducing the amount of gas released into the working space during mining operations. Conversely, the method focused on altering the gas flow path involves the construction of boreholes or roadways that connect with existing gas flow channels. Through the application of negative pressure in the drainage system, gas is drawn into the system,

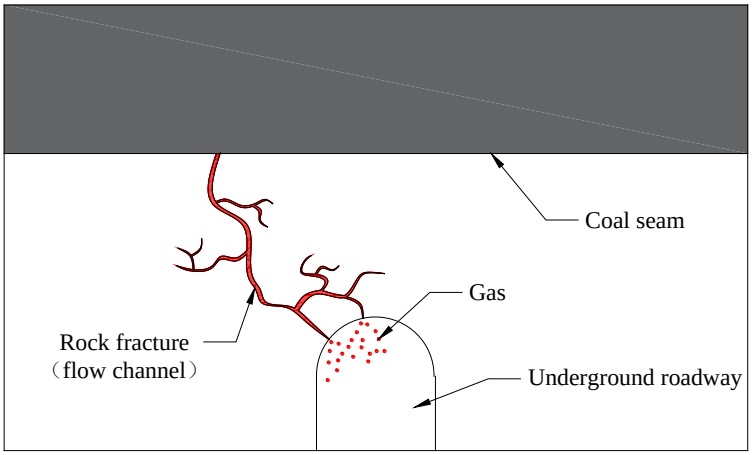
thereby achieving the objective of redirecting the gas flow and intercepting gas before it enters the working space.

Gas drainage interception technology is fundamentally a method for gas drainage. This technology primarily achieves its goal of intercepting gas by altering the gas flow path and is predominantly utilized during mining face operations and roadway excavation processes. One of the key advantages of gas drainage interception technology is its adaptability to the confined conditions of underground working environments. It effectively intercepts gas entering the working space without necessitating large-scale construction of drainage boreholes to eliminate gas sources. This approach minimizes disruptions to mining operations, reduces construction complexity, and lowers economic costs, thereby enhancing the safety of mining activities.

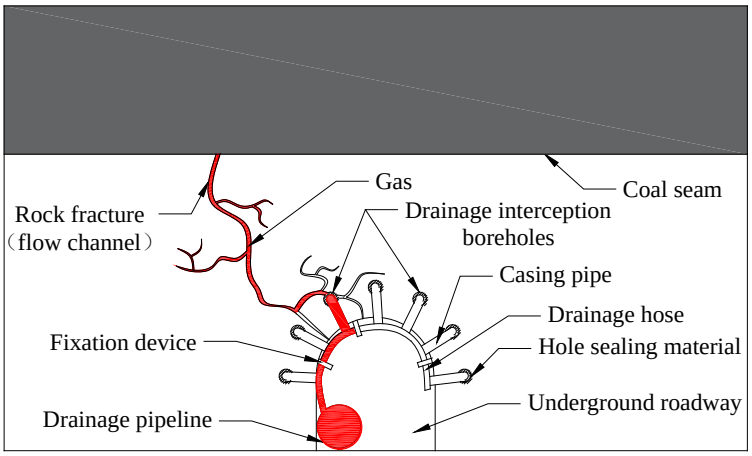
2.2 Technological principles

The gas drainage interception technology primarily involves the construction of drainage interception boreholes situated between the gas source and the working space, thereby artificially creating a negative pressure area that is connected to the gas flow channel. According to the principle of fluid potential, fluid naturally flows from areas of high potential to those of low potential. The application of negative pressure disrupts the original dynamic equilibrium state of each medium within the gas flow channel, facilitating the introduction of gas into the mine's drainage system. Consequently, the original flow path of gas, defined as gas source → flow channel → working space, is altered to gas source → flow channel → drainage system via the drainage interception borehole. During this process, the gas within the coal seam migrates differently through the coal seam and pores, utilizing seepage and diffusion. Under the influence of its own pressure and concentration gradients, the gas rapidly migrates through the fractures in the coal and rock mass, forming a gas flow field. At this stage, the gas movement in the coal seam predominantly

exhibits non-Darcy seepage behavior, resulting in a continuous decrease in the gas content of the coal seam, particularly the free gas content. Overall, this technology does not require the direct construction of gas drainage boreholes to reduce or eliminate the gas source in the coal seam; instead, it simply intercepts gas within the flow channel to alter its flow path. For instance, in roadway excavation, the gas drainage interception technology can be employed to intercept gas migrating from adjacent coal seams into the roadway working space. It is assumed that gas from the coal seam above the roadway enters through rock fractures, potentially compromising safe construction. To mitigate this, an drainage interception borehole can be positioned above the roadway, capturing the gas before it can infiltrate the roadway, thus effectively achieving gas interception. The relevant gas interception diagram is illustrated in Fig. 2.



(a)



(b)

Fig. 2 Gas drainage interception boreholes interception gas. (a) Gas flow path when not intercepted. (b) Gas flow path after being intercepted.

2.3 Technical application process

The effectiveness of gas drainage interception technology hinges on the strategic placement of gas drainage interception boreholes in relation to the gas flow channel. This necessitates thorough research and analysis prior to the construction of any boreholes. Taking the roadway depicted in Fig. 2 as an example, which remains connected to the coal seam above via rock fractures, it is imperative to first assess the geological conditions surrounding the roadway. Various detection methods, including direct current technology, transient electromagnetic technology, and ground-penetrating radar, should be employed [23-27]. The goal is to delineate the distribution range of the rock fractures (gas flow channels) as accurately as possible.

Subsequently, it is essential to identify the primary gas source. In the scenario illustrated in Fig. 3, the gas source is clearly the coal seam situated above the roadway. However, if the working space is positioned between multiple coal seams, specific technical measures must be implemented to identify and analyze the predominant gas source to facilitate targeted interception strategies. This can be achieved through a comparative analysis of parameters such as gas pressure, gas content, gas composition, and hydrocarbon isotopes [28-29].

Additionally, to prevent the direct connection of the drainage interception borehole to the roadway, which could lead to substantial air influx and compromise gas interception efficiency, it is crucial to examine the extent of the surrounding rock's loose circle formed post-roadway excavation. This analysis ensures that the effective drainage interception section of the borehole remains outside the loose circle’s range. Techniques such as numerical simulation or field measurements can be employed to assess the loose

circle of the surrounding rock [30-31].

Building upon the findings from the aforementioned research and analyses, the configuration of the gas drainage interception boreholes is determined. The layout must optimize the gas interception effect, which can include either single-layer or multi-layer borehole arrangements depending on the specific circumstances. Finally, the effectiveness of the gas drainage interception technology should be evaluated and refined. In summary, the application process for gas drainage interception technology in roadways between coal seams is shown in Fig.3:

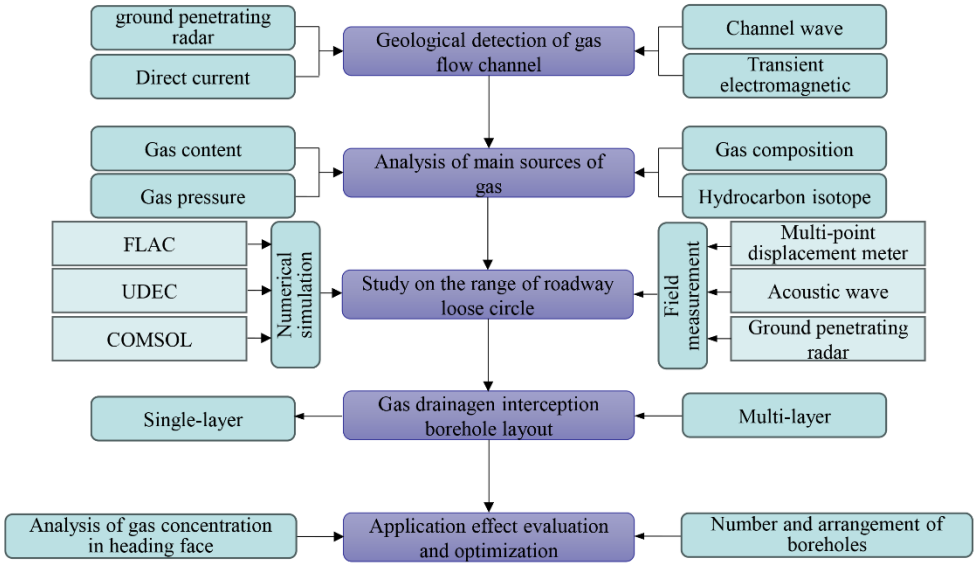


Fig. 3 Application process of gas drainage interception technology

3. Engineering application

3.1 Engineering background

The Liu Jia Liang Coal Mine is located in Xinzhou City, Shanxi Province, China, and is classified as a high-gas mine. It primarily extracts from the 2# and 5# coal seams. The 221 East Wing Track Roadway serves as a rock roadway situated in the lower section of the 221 Mining Area. Flanking this roadway on both sides are the 221 East Wing Belt Roadway to the left and the 221 East Wing Return-Air Roadway to the right. These adjacent roadways are coal roadways and are positioned 16 meters above the 221 East

Wing Track Roadway within the 2# coal seam. The underground layout of the 221 East Wing Track Roadway is illustrated in Fig. 4.

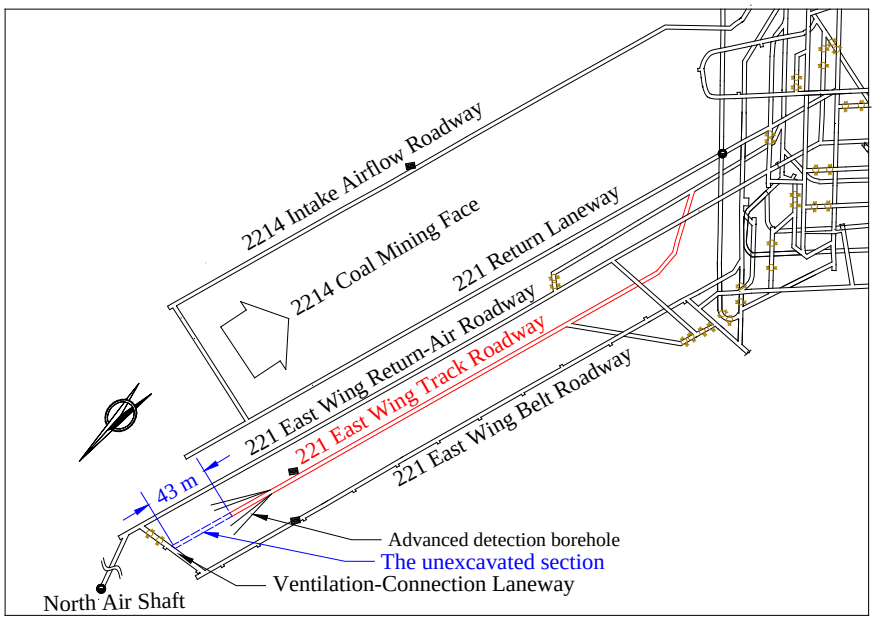


Fig. 4 Underground location of 211 East Wing Track Roadway

It can be seen from Fig.4 that the continuous excavation of the 221 East Wing Track Roadway can connect it with the front Ventilation-Connection Laneway, and then form a complete ventilation system in the east wing of the 221 Mining Area. The system is mainly composed of 221 East Wing Track Roadway, 221 East Wing Belt Roadway and 221 East Wing Return-Air Roadway. On this basis, on the west side of 221 East Wing Belt Roadway, along the direction perpendicular to the roadway, the mining roadway is gradually excavated and the coal mining face is formed, thereby enabling the mining of coal seams on the west side of the 221 East Wing Belt Roadway.

During the excavation of the 221 East Wing Track Roadway, specifically at the mileage mark of 680 meters, a minor influx of water and gas was observed at the excavation face following blasting operations. The water influx was primarily attributed to residual blast holes and blasting fractures located in the middle and lower sections of the excavation face, while the gas emission was mainly channeled through residual

blast holes and fractures found in the upper part of the excavation face. Observations of the rock strata at the excavation face revealed no significant alterations in their orientation. However, the blasting activities did induce a number of residual blast holes and numerous blasting cracks, which subsequently facilitated the flow of gas and water into the roadway's working space.

To mitigate the risk of gas accumulation at the excavation face, the residual blast holes and blasting cracks were temporarily sealed using concrete plugging techniques. Investigations involving construction personnel and review of construction records indicated no irregularities prior to the blasting operation. Consequently, it is likely that the observed water and gas influx at the excavation face resulted from the blasting, which generated cracks in the rock mass ahead of the excavation and is associated with the pre-existing water influx and gas emission pathways within the surrounding rock mass.

Furthermore, laboratory analyses of collected water samples confirmed that the water emanating from the excavation face originates from sandstone fissure water located on the roof of the 2# coal seam. Additionally, measurements of water flow in the ditch of the 221 East Wing Track Roadway indicated that the total water inflow at the excavation face ranged between 15 to 20 m^3/h. Given that the rock strata do not contain gas, it can be inferred that the gas present at the excavation face is likely sourced from the coal seams situated above or below the 221 East Wing Track Roadway. Relevant geological data illustrating the distribution of coal and rock layers surrounding the 221 East Wing Track Roadway is presented in Fig. 5.

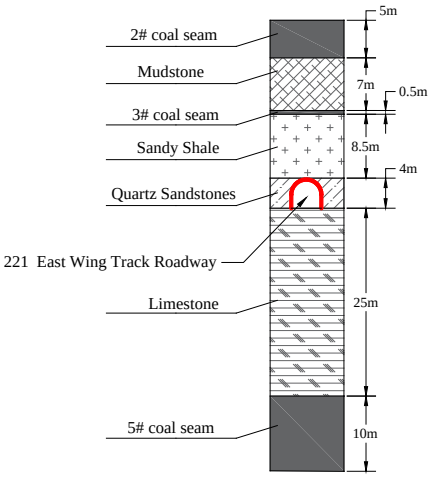


Fig. 5 Distribution of coal and rock layers around the roadway

3.2 Geological exploration

(1) Transient electromagnetic detection

To investigate the concealed geological formations within the area extending from the excavation face of the 221 East Wing Track Roadway to the Ventilation-Connection Laneway ahead, transient electromagnetic technology was employed. Detection was conducted in three distinct orientations within the 221 East Wing Track Roadway. Specifically, the conversion angle method was utilized when applying the transient geomagnetic method to examine the geology in front of the excavation face [32]. This method involved measuring inclination angles of −45°, 0°, and 45° between the coil device and the excavation face to assess the geological conditions below, in front of, and above the excavation face（Fig.6）, respectively. The transient electromagnetic detection equipment used in the mine was the YCS3000 model, which operates at an emission current of 2 A and has a coil side length of 2 × 2 m. The resulting advanced resistivity profile obtained from the transient electromagnetic detection is illustrated in Fig. 7.

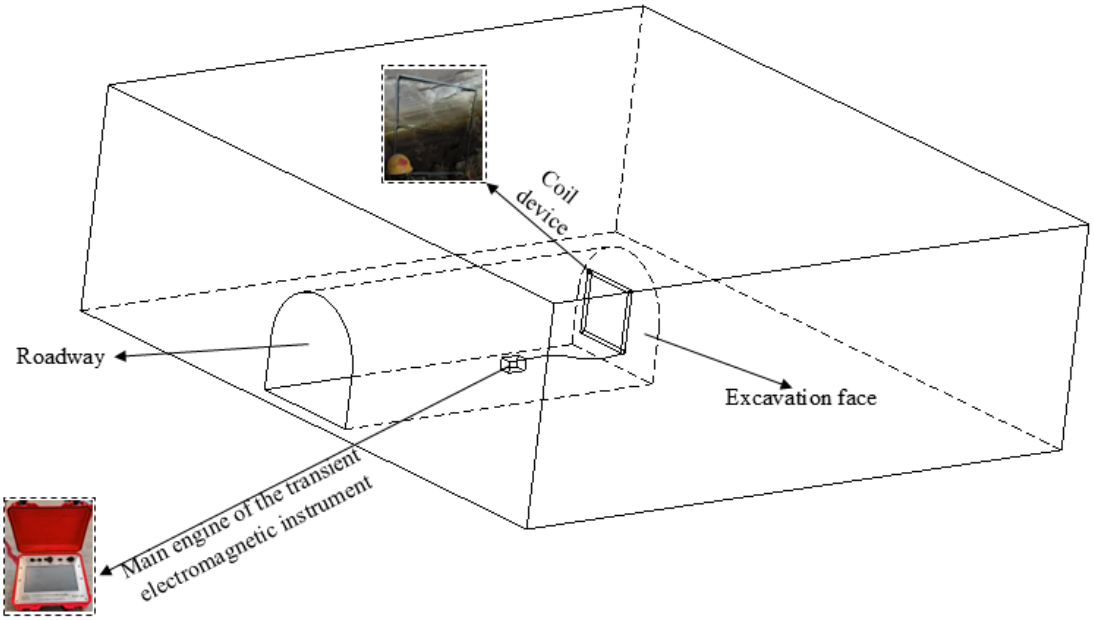
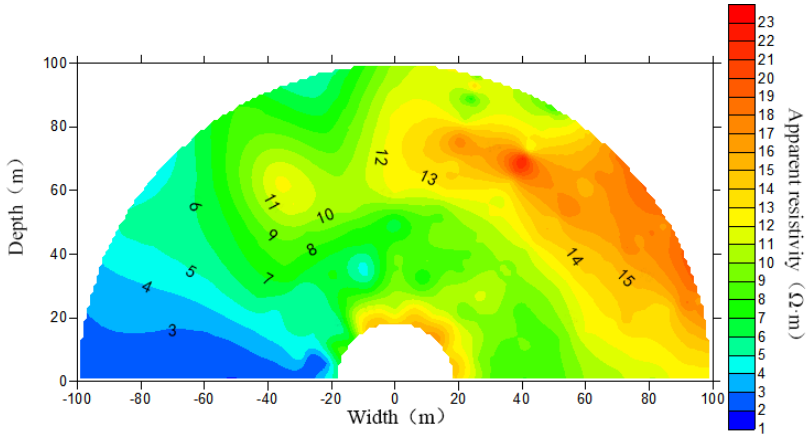
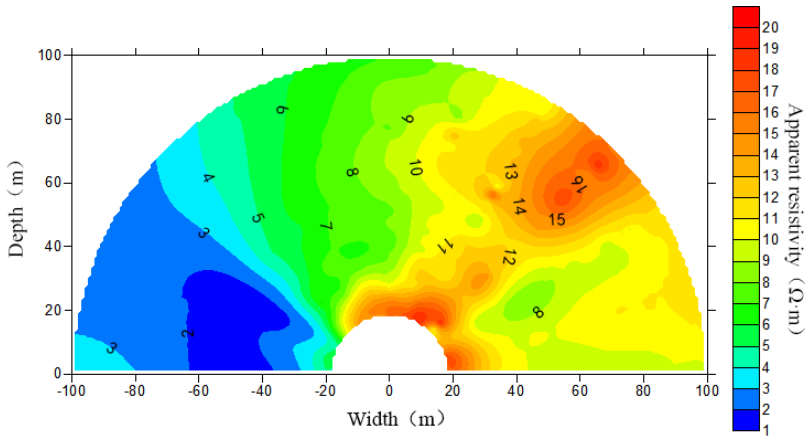


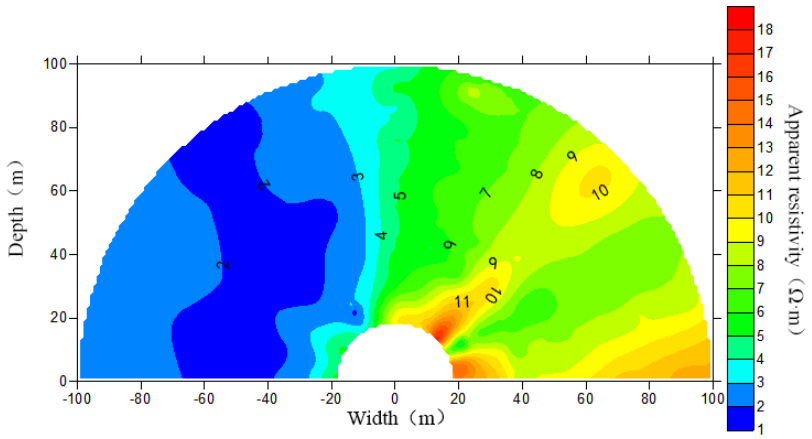
Fig.6 Layout of transient electromagnetic instrument in roadway. In the figure, the angle between the coil device and the excavation face is 0 °, that is, the plane formed by the coil is parallel to the excavation face.



(a)



(b)



(c)

Fig. 7 Cross-section of transient electromagnetic advanced exploration apparent resistivity. (a) 45° oblique upward direction. (b) horizontal direction. (c) 45° oblique downward direction.

Fig. 7 clearly illustrates that the apparent resistivity in the three examined directions exhibits a notable low apparent resistivity phenomenon on the left side of the roadway. This observation indicates the presence of fissures and high water content in the rock strata within this area. Furthermore, the apparent resistivity contour map reveals that the rock fractures between 40 and 60 m on the left side of the roadway are particularly well-developed. Analysis suggests the potential existence of a weak fracture zone in this region, characterized by a downward trend in elevation and an expanding area. Additionally, as the detection area descends from the upper section of the roadway, the low apparent resistivity zone enlarges, indicating a gradual increase in water content within the rock fractures from the top to the bottom in front of the roadway.

(2) Engineering geologic drilling

To further assess the geological conditions in front of the excavation face of the 221 East Wing Track Roadway, a total of nine boreholes were designed and constructed at the excavation face. The layout of these boreholes is depicted in Fig. 8, and the pertinent construction parameters are detailed in Table 1. The

geological drilling utilized a ZDY2000S coal mine drilling rig, featuring a supporting drill pipe diameter of 65 mm.

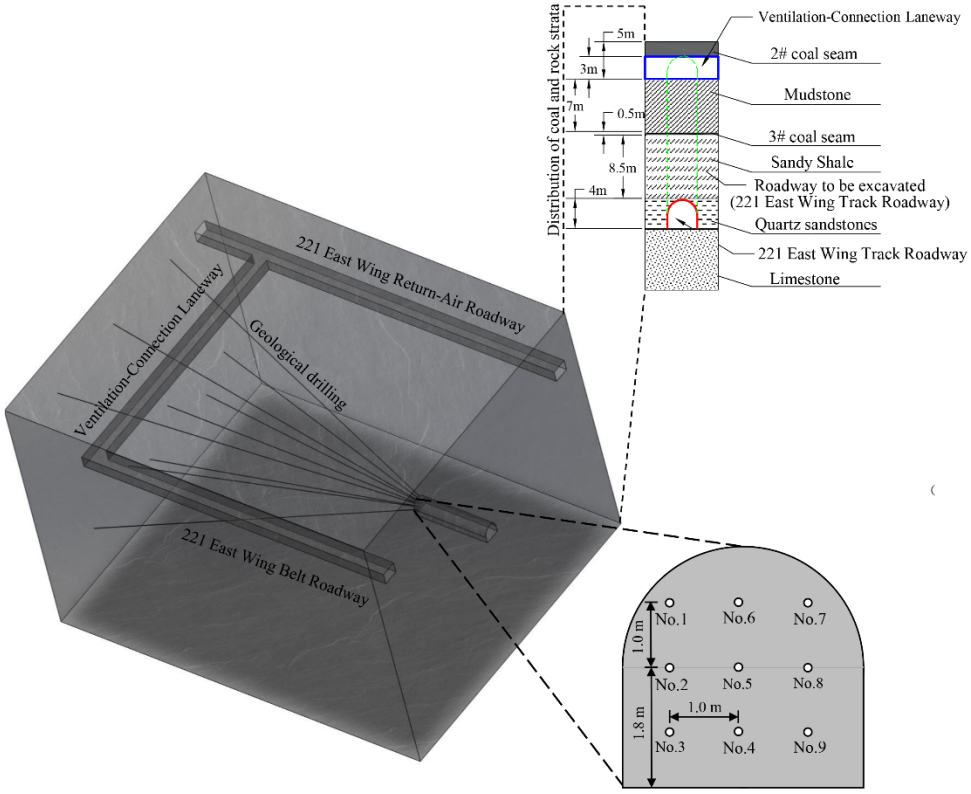


Fig.8 Layout of geological boreholes

Table 1. Geological boreholes construction parameters

Number	Azimuth/°	Dip angle/°	Diameter/mm	Drilling depth/m
No.1	348	25	75	90
No.2	348	0	75	70
No.3	348	-20	75	90
No.4	18	-20	75	90
No.5	18	0	75	70
No.6	18	25	75	90
No.7	28	25	75	90

No.8	28	0	75	70
No.9	28	-20	75	90

To mitigate gas accumulation in the working face due to communication between borehole construction and the surrounding rock fractures, a "three prevention" device is employed during the construction process. Additionally, when constructing the first borehole (Borehole 1), gas pressure measurements are taken within the borehole. Construction is halted at a depth of 30 m, at which point the borehole is sealed, and a pressure gauge is installed. Following the pressure measurement, construction resumes until the designated depth is reached. Concurrently, gas pressure in the 2# and 3# coal seams is measured during the construction of Boreholes No.6 and No.7, respectively. Coal samples from these seams are collected throughout the construction process to ascertain gas content. The geological borehole construction records are presented in Table 2.

Table 2 Geological drilling construction records

Number	Original construction records
No.1	Gas is gushing, with no water influx or sudden changes in rock layers.
No.2	Water and gas are gushing, with no sudden changes in rock layers.
No.3	A significant amount of water is gushing; gas is encountered after drilling into the coal seam. No sudden changes in the rock layer are observed, and drilling to a depth of 40-50 meters yields crushed stones with a particle size of 10-30 mm.
No.4	Water is gushing, and gas is encountered after drilling into the coal seam, with no sudden changes in rock layers.
No.5	Water is gushing, with no gas influx or sudden changes in rock layers.
No.6	Gas is gushing, with no water influx or sudden changes in rock layers.

No.7	A large volume of gas is gushing, with no water influx or sudden changes in rock layers.
No.8	Water is gushing, with no gas influx or sudden changes in rock layers.
No.9	Water is gushing, and gas is encountered when drilling into the coal seam, with no sudden changes in rock layers.

The absence of abrupt changes in rock layers across the entire detection range, as shown in Table 2, indicates that there are no significant geological structures, such as faults or folds, present in this area. However, the emergence of crushed stones with a particle size of 10-30 mm in borehole No.3, encountered at a depth of 40-50 m, coupled with the results from transient electromagnetic detection, suggests the presence of a weak fracture zone within the rock matrix. Furthermore, the observed water and gas emissions from each borehole imply that fractures exist in the rock mass in front of the excavation face. Additionally, analysis of the water sample measurements indicates that these fractures are likely associated with the roof sandstone of the 2# coal seam, extending into the 3# coal seam. When evaluating roadway water inflow, it is evident that the inflow from boreholes on the left side of the roadway is significantly greater than that from the right side, and the inflow on the lower side exceeds that on the upper side. This discrepancy may be attributed to the elevation of the boreholes and the enhanced water richness of the rock fractures beneath the roadway.

In summary, integrating the findings from transient electromagnetic detection and engineering geological drilling, it is inferred that numerous rock fractures are present in the rock mass in front of the excavation face of the 221 East Wing Track Roadway. And in the range of 40-60 m on the left side of the roadway, it is very likely that there are bad geological bodies. Moreover, the analysis of gas emissions from the entire excavation face indicates that the gas flow channel connected to the excavation face is predominantly located in the upper front region.

3.3 Gas source analysis

Under normal conditions, rock formations typically do not contain gas. Therefore, the gas present at the excavation face of the 221 East Wing Track Roadways is primarily sourced from the adjacent coal seams. Additionally, the water gushing from the excavation face originates from the sandstone fissure water located in the roof of the 2# coal seam. The rock fractures connect the sandstone to both the 2# and 3# coal seams. Measurements taken during the geological borehole construction revealed a gas pressure of 0.62 MPa within the fractures, while the gas pressures in the 2# and 3# coal seams were recorded at 0.15 MPa and 0.18 MPa, respectively. These values are significantly lower than the gas pressure observed in the fractures in front of the excavation face. Furthermore, since both the 221 East Wing Return-Air Roadway and the 221 East Wing Belt Roadway were constructed within the 2# coal seam without encountering gas anomalies during the process, it is plausible that the primary gas source is the 5# coal seam located beneath the 221 East Wing Track Roadways.

To accurately identify the main gas source at the excavation face, we employed a comparative analysis of gas parameters and gas compositions. This involved measuring and comparing the gas pressure, gas content, and gas composition of the rock fractures in front of the excavation face with those of the adjacent coal seams.

(1) Measurement of Gas Parameters in Adjacent Coal Seams

To mitigate the influence of water on the determination of gas parameters for the 5# coal seam, a pressure-measuring borehole with a diameter of 75 mm was drilled to the 2#, 3#, and 5# coal seams, respectively, at a distance of 150-155 m from the excavation face in the 221 East Wing Track Roadway, as illustrated in Fig. 9. During the borehole construction process, coal samples from the three seams were collected, and the gas pressure and content for each seam were measured. The results of these

measurements are presented in Table 3.

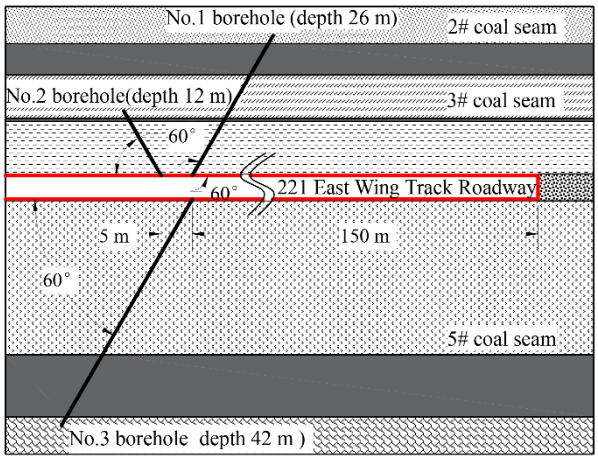


Fig.9 Cross section diagram of pressure measuring boreholes

Table 3. Determination results of gas content and gas pressure in each coal seam

Coal seam	Measurement location	gas content (m^3/t)	gas pressure (MPa)
2#	150 m away from the excavation face	3.26	0.16
3#	155 m away from the excavation face	3.80	0.18
5#	150 m away from the excavation face	6.78	0.66

Table 3 indicates that the gas pressure value of the 5# coal seam is 0.66 MPa, which is comparable to the gas pressure of 0.62 MPa recorded in the rock fractures located in front of the excavation face. The gas pressure values for the 2# and 3# coal seams remain consistent with those obtained from previous geological boreholes, all falling within the range of 0.15 to 0.18 MPa.

(2) Determination of Gas Composition in Adjacent Coal Seams

To further elucidate the gas source at the excavation face of the 221 East Wing Track Roadway, gas samples were collected from each adjacent coal seam following the measurement of gas pressures. These gas samples were collected by using a gas sample collection bag (capacity 1 L) during the removal of the gas pressure gauge, and one gas sample was collected from each coal seam. Additionally, gas samples

from the fractures in front of the excavation face were collected and measured. After the gas sample was collected, it was sent to the laboratory, and the components of each gas sample were determined by gas chromatograph. The results of these measurements are presented in Fig. 10.

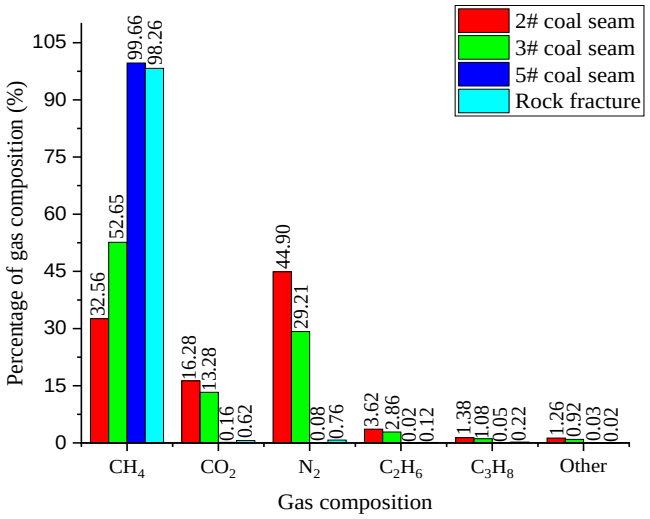


Fig.10 Gas composition determination results

Fig. 10 Illustrates that methane (CH_4) constitutes 32.56% of the gas in the 2# coal seam, 52.65% in the 3# coal seam, 99.66% in the 5# coal seam, and 98.26% in the rock fractures in front of the excavation face. Notably, the CH_4 concentration in the gas from the 5# coal seam is the highest, closely resembling the CH_4 concentration observed in the rock fractures.

(3) Comprehensive Analysis of Gas Sources

The measurement results of gas parameters and gas compositions in the adjacent coal seams and rock fractures in front of the excavation face of the 221 East Wing Track Roadway indicate that the gas pressure values and CH_4 proportions in the 2# and 3# coal seams are significantly lower than the corresponding values in the fractures. In contrast, the correlation value of the 5# coal seam is more aligned with the fracture measurements. Furthermore, both the 221 East Wing Return-Air Roadway and the 221 East Wing Belt Roadway are situated within the 2# coal seam, where the gas concentration at the excavation face remained below 0.30% throughout the excavation process, even in the absence of gas drainage measures.

Additionally, according to coal uncovering data provided by the mine, no gas anomalies were detected when the 3# coal seam was exposed in other roadways, suggesting that the 2# and 3# coal seams are less likely to be the primary gas sources. Consequently, gas drainage measures must be implemented during the excavation of the 5# coal seam. Typically, the gas drainage strategy combines pre-mining drainage with concurrent drainage, with the pre-mining drainage period for the coal seam usually exceeding six months. Thus, the 5# coal seam possesses the potential to serve as a stable gas supply source. Comprehensive analysis concludes that the gas present in the excavation face of the 221 East Wing Track Roadway primarily originates from the 5# coal seam.

3.4 Numerical simulation of roadway loose circle range

According to the revised excavation plan for the roadway, a slope of 20° will be maintained towards the Ventilation-Connection Laneway. It is imperative to avoid large-scale construction of gas drainage boreholes in the roadway directed towards the 5# coal seam in order to rapidly mitigate the gas supply source. To reduce the impacts associated with mining replacement, construction complexities, and economic costs, the gas drainage interception technology has been selected for intercepting gas inflow into the roadway. During the application of this technology, the drainage interception borehole connects to the surrounding rock fractures, which may also link to the roadway. While intercepting gas flowing into the roadway, air from within the roadway can also be drawn into the borehole, potentially affecting the interception efficiency of the drainage system. Therefore, it is essential to effectively manage the distance between the drainage interception borehole and the surrounding fractures. Consequently, prior to constructing the drainage interception borehole, it is necessary to investigate the fracture range developed in the surrounding rock mass following roadway excavation.

Upon excavation of the roadway within native rock, the original stress equilibrium of the surrounding

rock is disrupted, resulting in stress redistribution. During this process, stress concentration occurs in the tangential direction of the roadway. When the concentrated stress surpasses the diminished rock strength, damage and expansion of the surrounding rock can ensue, ultimately forming a circular damage zone known as the loose circle of roadway surrounding rock [33]. If the drainage interception borehole intersects with the loose circle or is positioned within this zone, it will come into direct contact with the air in the roadway. This scenario can lead to significant air influx into the drainage interception borehole, thereby severely compromising its interception efficiency and reducing the overall drainage performance. To ascertain the extent of the loose circle of surrounding rock formed post-roadway construction, FLAC3D numerical simulation software was utilized. In this context, the plastic zone denotes the area where material experiences plastic deformation after reaching its yield limit, effectively delineating the loose circle's extent [34]. In accordance with the specific conditions of the 221 East Wing Track Roadway（The width of the roadway is 4.0 m, the height of the arch foundation is 1.5 m, and the radius of the semi-circular arch is 2.0 m, and the roadway support method is anchor spray）, a model measuring X×Y×Z = 10 m × 70 m × 50 m was established, as illustrated in Fig. 11. The model employs a plane strain analysis with a Mohr-Coulomb constitutive model. The upper boundary is defined as free, and a stress load of 13.92 MPa is applied based on the burial depth. Displacement boundary conditions are imposed at the bottom and surrounding areas of the model to restrict movement. The physical and mechanical parameters for each coal seam in the model are summarized in Table 4.

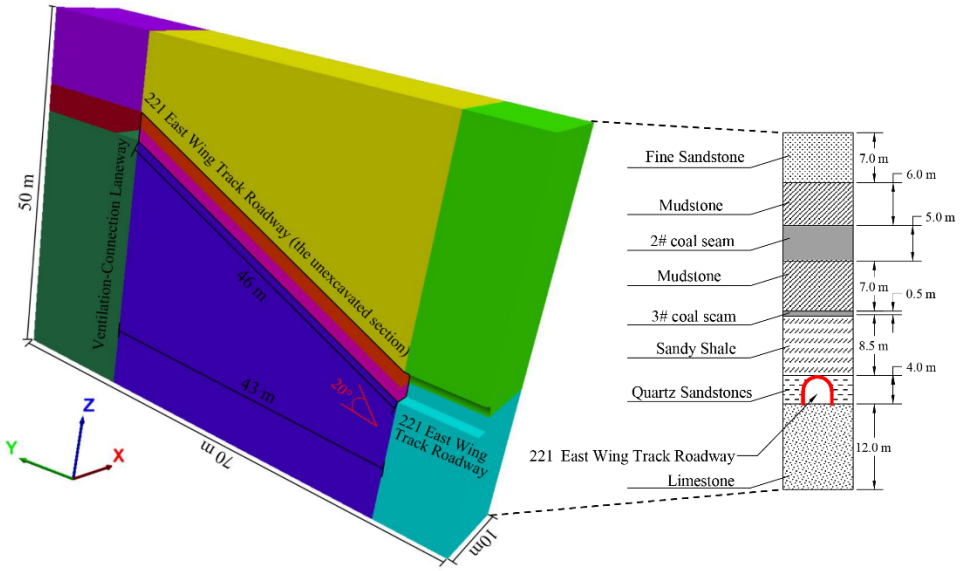


Fig.11 Numerical calculation model

Table 4. Physical and mechanical parameters of coal and rock layers

Rock formation	Density (Kg/m^3)	Tensile strength (MPa)	Cohesion (MPa)	Shear modulus (GPa)	Bulk modulus (GPa)	Internal friction angle (°)
Fine Sandstone	2620	2.92	3.26	2.10	3.16	24
Mudstone	2410	2.68	2.82	2.34	3.10	26
2# coal seam	1310	0.82	0.42	1.40	3.52	32
3# coal seam	1350	0.80	0.45	1.42	3.60	30
Sandy Shale	2620	2.25	3.56	3.20	3.86	28
Quartz Sandstones	2680	2.76	3.76	3.30	4.18	30
Limestone	2650	1.80	3.08	2.68	3.26	24

Based on the actual excavation rate of the roadway, the model is developed with an excavation step distance of 1.0 m. Following the excavation, damage and failure occur in the surrounding rock, resulting in the formation of a loose circle around the roadway. The extent of this loose circle can be represented by

the size of the plastic zone within the computational model [35]. Consequently, after the roadway excavation is completed, a distribution map of the plastic zone in the surrounding rock is extracted, and a representative distribution map is presented in Fig. 12.

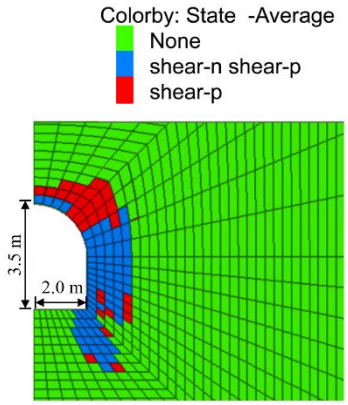


Fig.12 Distribution of plastic zone in roadway surrounding rock

Fig. 12 illustrates that during the subsequent excavation of the 221 East Wing Track Roadway, the maximum damage to the surrounding rock occurs at the bottom corner of the roadway, with an extent reaching up to 2.30 m. The damage on the sides of the roadway ranks second, with a maximum extent of 1.70 m, while the damage at the top of the roadway is comparatively smaller, measuring 0.65 m. This distribution of damage in the surrounding rock is influenced by the shape of the roadway cross-section and the properties of the surrounding rock mass. Excavation activities alter the stress state within the surrounding rock, leading to stress redistribution. Notably, at the corners of the roadway, geometric changes result in pronounced stress concentration phenomena. In trapezoidal section roadways, stress concentration is more likely to occur at the corners, whereas circular or elliptical roadways tend to disperse stress more effectively, thereby reducing the likelihood of stress concentration [36]. Consequently, the loose circle of the surrounding rock exhibits a greater damage range at the bottom corner and a smaller damage range at the top. Based on this analysis, the loose circle range of the 221 East Wing Track Roadway is determined to be between 0.65 m and 2.30 m.

3.5 Drainage interception borehole layout

Given that the gas at the excavation face primarily originates from the 5# coal seam, it is essential to construct drainage interception boreholes between the 5# coal seam and the roadway being excavated to effectively intercept gas. However, due to constraints related to working space and challenges in accurately determining the distribution range of rock fractures, this study suggests that it is more reliable and safer to arrange the drainage interception boreholes around the roadway. To minimize the influx of air from the roadway into the drainage interception borehole, which could adversely affect interception efficiency, this paper introduces a dual drainage interception technology characterized by high and low negative pressure. This approach involves installing two concentric layers of drainage interception boreholes around the roadway. The outer layer of drainage interception boreholes is situated further from the roadway contour and operates under high negative pressure (not less than 13 kPa, here is 28 kPa) primarily to intercept gas. Conversely, the inner layer of drainage interception boreholes is positioned closer to the roadway contour and functions under low negative pressure (between 4 kPa and 13 kPa, here is 10 kPa) to supplement gas interception and reduce the volume of air entering the borehole from the roadway.

Based on the configuration of the high and low negative pressure dual drainage interception boreholes, along with the distribution characteristics of the surrounding rock's loose circle, relevant drainage interception boreholes (with a diameter of 94 mm) were installed in both the 221 East Wing Track Roadway and the Ventilation-Connection Laneway. The layout parameters for each drainage interception borehole are detailed in Table 5, while the spatial distribution of each drainage interception borehole is depicted in Fig. 13.

Table 5. Construction parameters of each drainage interception borehole

Number	Azimuth	Dip	Drilling	Drainage	Number	Azimuth	Dip	Drilling	Drainage

	°	angle °	depth m	method		°	angle °	depth m	method
No.1-1	16.5	18.7	65.0		No.2-2	15.7	17.9	67.6	
No.1-2	16.5	18.7	65.0		No.2-3	15.7	18.3	67.8	
No.1-3	16.6	19.3	65.0		No.2-4	16.0	19.1	68.2	
No.1-4	16.9	19.8	65.5		No.2-5	16.6	19.8	68.8	
No.1-5	17.5	20.2	66.0		No.2-6	17.5	20.2	69.3	
No.1-6	18.1	20.4	66.3		No.2-7	18.4	20.4	69.7	
No.1-7	18.8	20.4	66.6		No.2-8	19.4	20.2	70.1	
No.1-8	19.4	20.2	66.7		No.2-9	20.2	19.8	70.2	
				High					Low
No.1-9	19.9	19.8	66.7		No.2-10	20.8	19.7	70.2	
				negative					negative
No.1-10	20.3	19.3	66.5		No.2-11	21.2	18.3	70.0	
				pressure					pressure
No.1-11	20.4	18.7	66.5		No.2-12	21.2	17.9	69.8	
				drainage					drainage
No.1-12	20.4	18.7	66.5		No.2-13	21.2	17.9	69.8	
				(28 kPa)					(10 kPa)
No.1-13	198.4	-23.3	58.2		No.2-14	198.4	-23.8	60.0	
No.1-14	198.4	-23.3	58.2		No.2-15	198.4	-23.8	60.0	
No.1-15	198.4	-23.3	58.2		No.2-16	198.4	-23.8	60.0	
No.1-16	198.4	23.3	58.2		No.2-17	198.4	-23.8	60.0	
No.1-17	198.4	-23.3	58.2		No.2-18	198.4	-23.8	60.0	
No.1-18	198.4	-23.3	58.2		No.2-19	198.4	-23.8	60.0	
No.1-19	198.4	-23.3	58.2		No.2-20	198.4	-23.8	60.0	
No.1-20	198.4	-23.3	58.2		No.2-21	198.4	-23.8	60.0	

No.1-21	198.4	-23.3	58.2	No.2-22	198.4	-23.8	60.0
No.1-22	198.4	-20.7	56.6	No.2-23	198.4	-23.8	60.0
No.1-23	198.4	-19.2	56.1	No.2-24	198.4	-21.3	57.9
No.2-1	15.7	17.9	67.6	No.2-25	198.4	-19.7	56.3

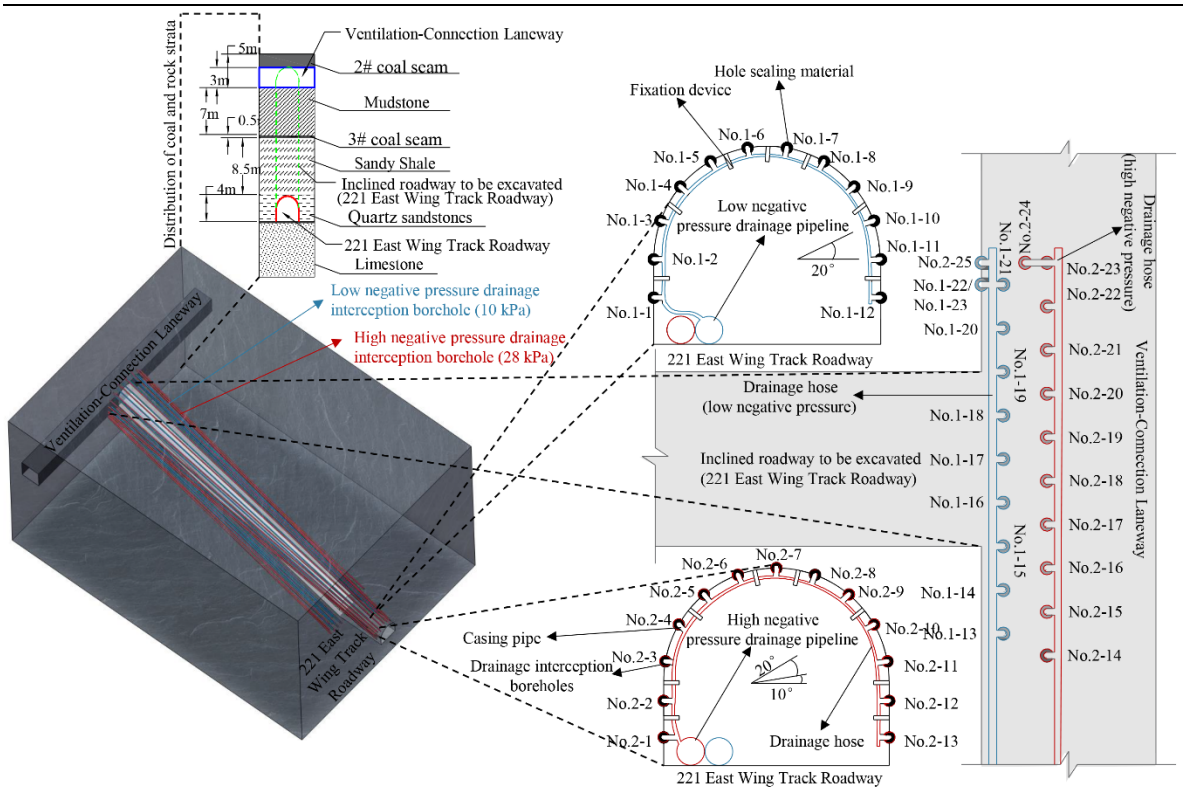
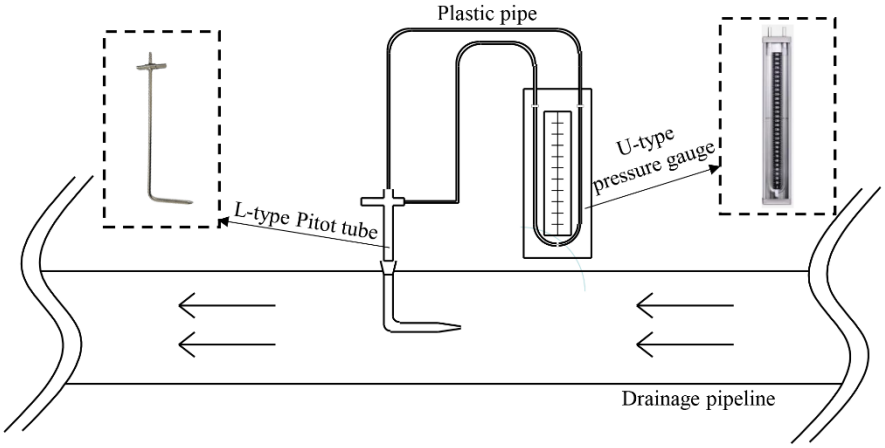


Fig.13 Layout of each drainage interception borehole

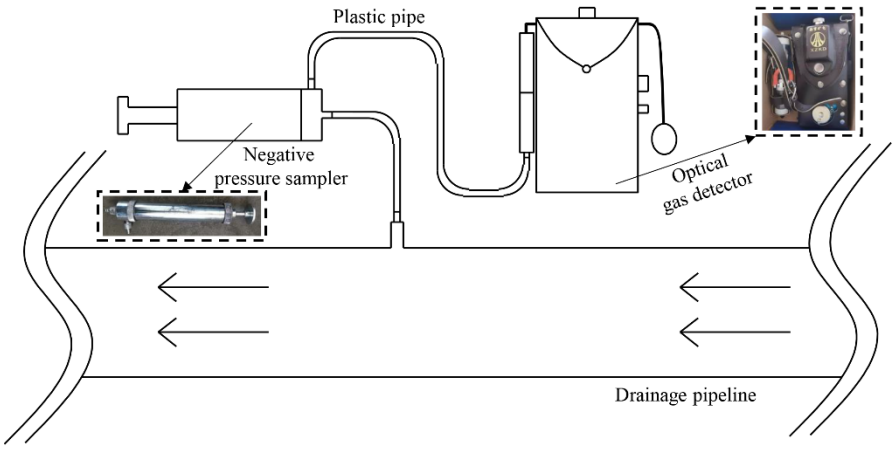
3.6 Analysis of gas interception effect

Upon completion of the construction and connection of high and low negative pressure dual drainage interception boreholes to the mine drainage pipe network, drainage parameters for each borehole were continuously monitored over a one-month period to assess the overall interception efficiency. Specifically, we measured both the drainage gas mixing volume and the gas concentration in each drainage interception borehole. The drainage gas mixing volume was primarily measured using a pitot tube (Fig.14 a), which captures the velocity pressure at the center point of the drainage tube, enabling the calculation of gas flow within the drainage tube [37]. Gas concentration was determined using a combination of a negative

pressure sampler and an optical gas detector (Fig.14 b). During measurement, the negative pressure sampler, connected via a plastic pipe, extracted gas from the drainage tube and directed it into the optical gas detector, which subsequently detected the gas concentration. Consequently, the pure gas drainage volume was calculated as the product of the gas mixing volume and the gas concentration. The data for each drainage interception borehole, detailing the pure gas flow volume, are presented in Fig.15.

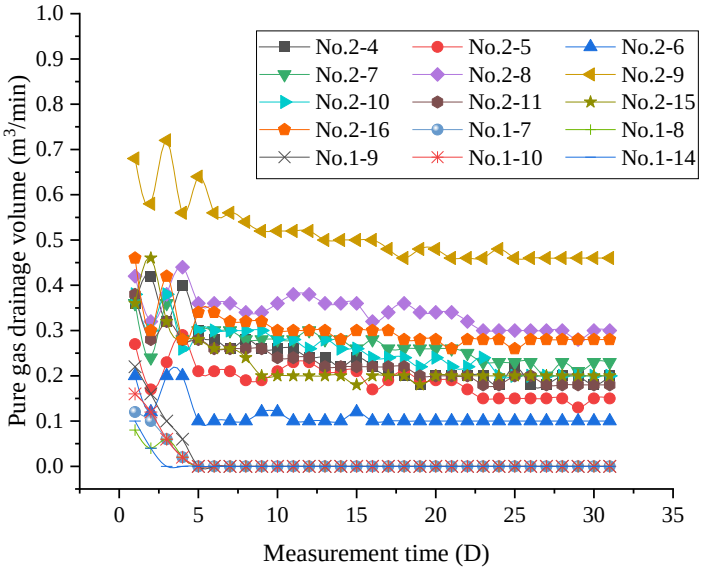


(a)



(b)

Fig.14 The connection between the measuring device and the drainage tube. (a) The connection between the pitot tube and the drainage tube; (b) The connection between the negative pressure sampler and the optical gas detector and the drainage tube.

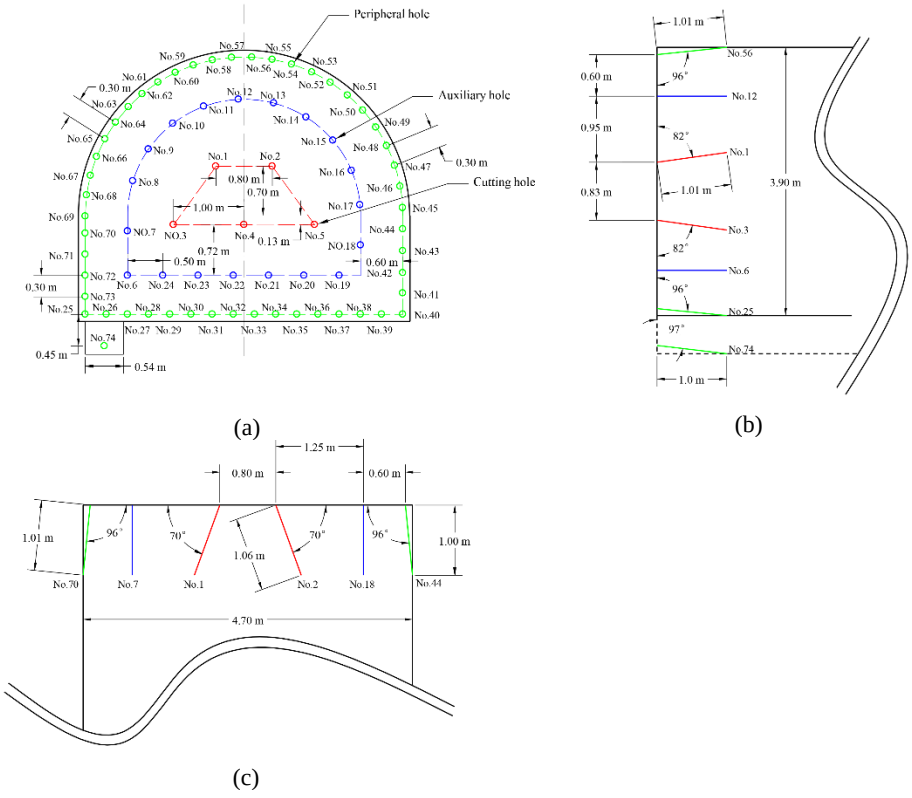


418

419 Fig.15 Variation law of pure gas drainage volume. The drainage gas concentration and drainage gas mixing amount of each
420 borehole are measured three times a day, and then the average value is calculated to obtain the pure gas drainage value of
421 each borehole on the day. The gas drainage pure volume is the product of gas mixing amount and gas drainage concentration.
422 In addition, different numbers of boreholes in the figure represent different drainage methods: No.1-x indicates that the
423 borehole adopts low negative pressure drainage; No.2-x indicates that the borehole adopts high negative pressure drainage.

424 Fig. 15 illustrates that the drainage purity from each drainage interception borehole exhibits
425 substantial fluctuations during the initial phase, a gradual decline in the mid-phase, and a stable trend in
426 the later phase. Specifically, the high negative pressure drainage interception boreholes (No.2-4 to No.2-
427 11) positioned at the top of the roadway within the 221 East Wing Track Roadway exhibit gas flow,
428 whereas gas presence is limited to boreholes No.2-15 and No.2-16 located on the right side of the
429 ventilation-connection laneway (in the direction of roadway excavation). This observation suggests that
430 the gas-bearing rock fractures associated with boreholes No.2-4 to No.2-11 likely lie outside the
431 interception range of the drainage interception boreholes situated at the bottom of the roadway, instead
432 connecting with the 5# coal seam in other regions and extending upwards to the top of the roadway.

Furthermore, gas was detected in only five low negative pressure drainage interception boreholes, with the drainage purity diminishing to 0 m^3/min within 2 to 4 days. This indicates that, following the stable operation of the drainage pipe network, the high negative pressure drainage interception boreholes effectively prevented gas from the surrounding fractures from infiltrating the low negative pressure drainage interception boreholes. Throughout the entire monitoring period, under conditions of full exposure of the rock strata at the excavation face, the gas concentration remained steady at 0.02%. The analysis confirms that the dual drainage interception technology—employing both high and low negative pressure—successfully intercepts gas from the surrounding fractures, thereby facilitating the initiation of trial excavation. During the trial excavation phase, a total of five blasting operations were conducted. The explosive used in the blasting excavation is the third-level coal mine allowable emulsion explosive, and the cartridge specification is φ35 mm × 250 mm ; the millisecond delay electric detonator is used to detonate, and the capacitive explosive is detonated. The blasthole arrangement is shown in Fig.16. Among them, the arrangement method for the cutting hole is the oblique (or angled) cutting method, and each blast hole adopts a forward continuous charge structure; The footage advance per blasting excavation in this roadway is 1.0 m.



448

449 Fig.16 Blasthole arrangement. (a) The front view of the blasthole layout in the working face, there were 5

450 cutting holes, 19 auxiliary holes and 55 peripheral holes. (b) The left view of the blasthole arrangement in

451 the working face, which only contains some blastholes that can reflect the length and inclination of

452 different blastholes; (c) The top view of the blasthole arrangement in the working face, which only contains

453 some blastholes that can reflect the length and dip angle of different blastholes.

454 In addition, the gas concentration in the return air flow at 10 m from the excavation face was

455 monitored before and after each blasting. The monitoring method is that before blasting excavation, two

456 symmetrically arranged rectangular grooves (the bottom of the rectangular groove is 2.0 m away from the

457 roadway floor) were excavated in the roadway section at a distance of 10 m from the excavation face.

458 Then the two gas detectors were fixed in the rectangular groove and covered with a rubber sleeve with

459 some through hole, and then the gas concentration near the excavation face during blasting excavation was

460 detected. The larger value of the two detectors' test result is taken as the final test result. In addition, in

order to facilitate the observation of the change of gas concentration before and after blasting excavation, this time only the maximum values monitored per minute are listed, as shown in Fig.17.

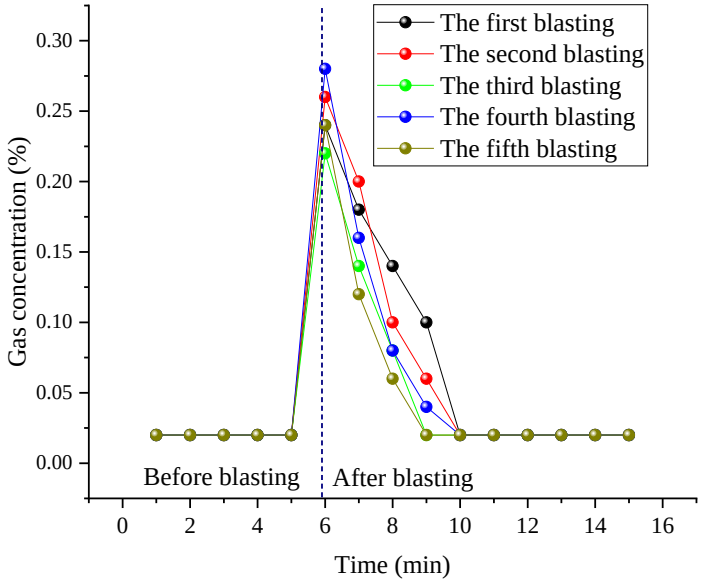


Fig.17 The variation law of gas concentration in the upper corner of roadway excavation face before and after blasting.

Fig. 17 demonstrates that the gas concentration near the excavation face exhibited a notable increase before and after the five blasting operations, rising from 0.02% prior to blasting to between 0.20% and 0.28% post-blasting. Nevertheless, the implementation of high and low negative pressure dual drainage interception boreholes facilitated a rapid restoration of the gas concentration to its original level of 0.02% within 2 to 4 minutes following the blasts. This indicates that, despite the blasting disturbances, a small volume of gas from the surrounding rock fractures can briefly penetrate the dual interception system of the high and low negative pressure drainage interception boreholes. The primary reason for this occurrence is that blasting induces instantaneous stress alterations and fragmentation of the rock mass at the excavation face, subsequently impacting the surrounding drainage interception boreholes. However, once the effects of the blasting disturbance dissipate, the dual drainage interception system is able to comprehensively intercept gas once again, thereby swiftly and effectively controlling the gas concentration

at the excavation face. This performance highlights that the interception capabilities of the high and low negative pressure dual drainage interception boreholes adequately satisfy the requirements for safe roadway excavation.

4. Discussion and limitation

4.1 Analysis of gas migration process

According to the detection results of the main gas circulation channels and the analysis results of the main sources of gas in the excavation face of the 221 East Wing Track Roadway, it can be seen that the gas in the excavation face of the roadway is migrated from the gas of the 5# coal seam below it to the gas circulation channel in front of the roadway through geological fissures, and finally enters the roadway through the blasting cracks in front of the excavation face. In order to facilitate the analysis of the migration process of gas from coal seam to roadway, we regard the coal seam and rock stratum connected by fractures as a closed combination. When this combination is not disturbed by external disturbance, the gas in coal seam will migrate to the interior of rock fissure and gradually reach the equilibrium state. When the coal-rock combination is disturbed by the external environment, so that its own cracks are connected to the external environment, the original gas balance state inside the coal-rock combination will be broken, and the gas will be quickly moved to the external environment under the influence of its own pressure gradient and concentration gradient, forming a gas flow field [38-39]. In this process, the dynamic balance between the adsorbed gas and the free gas in the coal seam is also broken. In the whole process of gas migration from the coal-rock combination to the external environment, the coal seam has always played the role of gas supply source, while the rock layer plays the role of gas circulation channel, continuously transporting gas to the external environment until the gas in the coal-rock combination reaches a new dynamic balance with the external environment.

4.2 Supplement measure

During the operation of the interception borehole designed to extract gas from the fractures surrounding the roadway, fissure water from the roof sandstone of the 2# coal seam inevitably enters the drainage pipeline along with the gas. This leads to an increasing accumulation of water within the pipeline, which significantly hampers the effective operation of the mine drainage system. To mitigate water accumulation in the drainage pipeline and minimize the labor burden on staff, multiple automatic water dischargers have been installed along the high and low negative pressure drainage pipelines within the roadway (Fig.18). Specifically, six automatic water dischargers have been placed on the high negative pressure drainage pipeline, while two have been installed on the low negative pressure drainage pipeline.

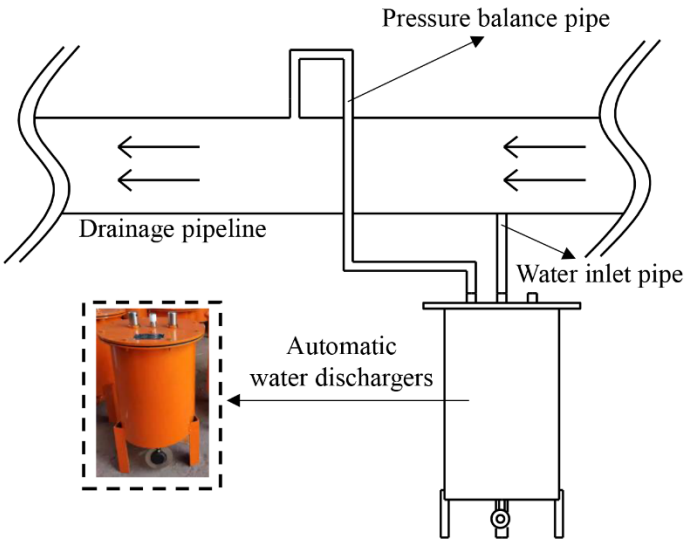


Fig.18 The connection between the automatic water discharger and the drainage pipeline

In parallel, to enhance the safety of the roadway excavation process, the excavation of the 221 East Wing Track Roadway is temporarily halted after approximately 13.0 m of advancement, and four penetrating holes are created in the excavation face. These holes connect the excavation face with the Ventilation-Connection Laneway, facilitating early exposure of the 3# coal seam, thereby accelerating gas emission from the coal seam. This strategy also serves to reduce ventilation resistance in the excavation

roadway and increases the gas dilution rate at the excavation face. The construction parameters for each penetrating borehole are detailed in Table 6, and their layout is illustrated in Fig. 19.

Table. 6 Construction parameters of each through-hole

Hole number	Azimuth/ °	Inclination/ °	Aperture/ mm	Drilling depth/ m
No.1	18.4	19.7	113	43.6
No.2	18.4	19.7	113	43.6
No.3	18.4	19.7	113	43.6
No.4	18.4	19.7	113	43.6

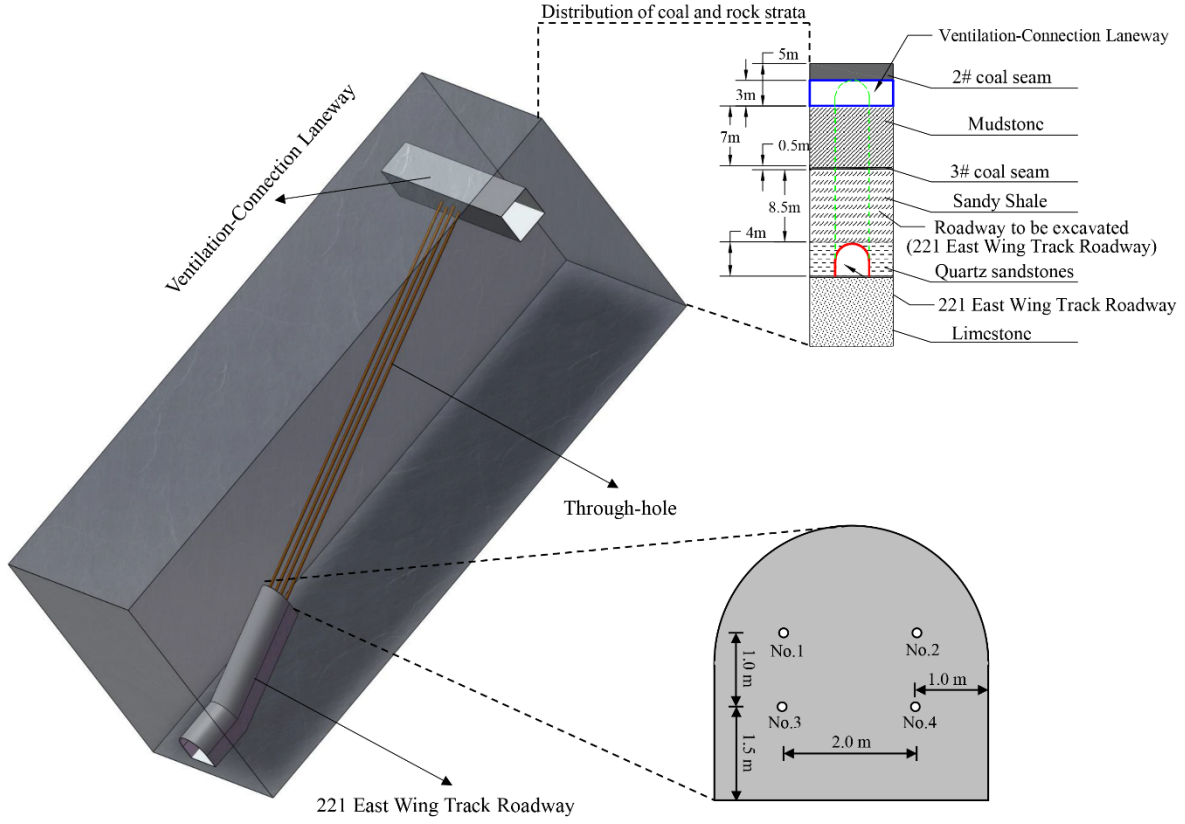


Fig.19 Distribution of through-hole

4.3 Limitation

Furthermore, the distribution of high and low negative pressure drainage interception boreholes around the roadway, along with the extent of the loose circle of the surrounding rock, indicates that the

low negative pressure drainage interception borehole is likely to make direct contact with the air in the roadway. This contact can significantly diminish its operational efficiency. Conversely, when the low negative pressure drainage interception borehole is positioned away from the loose circle of surrounding rock, the intention to reduce the blank zone—defined as the area unaffected by the drainage interception borehole—between the high and low negative pressure drainage interception boreholes necessitates an increase in the number of drainage interception boreholes, thereby escalating the overall workload. Consequently, it is imperative to optimize the layout of the drainage and interception boreholes to ensure both operational efficiency and a reduction in drilling construction. This optimization remains an area that has not yet been fully addressed. In addition, this paper only briefly analyzes the migration process of gas from coal seam to roadway, and lacks profound theoretical analysis. This gap represents a focal point for our future research endeavors.

5. Conclusion

This study utilizes the 221 East Wing track roadway of Liu Jia Liang Coal Mine as the experimental context. It systematically examines the application of gas drainage and interception technology, focusing on the gas flow pathways, primary gas sources, and the loose circle surrounding the roadway rock. The key findings of this research are as follows:

1) Gas drainage interception technology fundamentally constitutes a gas drainage method, where the technical principle revolves around altering the original gas flow path through the application of negative pressure. The implementation of this technology encompasses several critical processes, including the detection of gas flow channels, analysis of primary gas sources, determination of the loose circle range surrounding the roadway, strategic layout of gas drainage interception boreholes, and subsequent evaluation and optimization of application effectiveness.

2）By using different research methods, it is found that the gas channel of the excavation face of 221 East Wing Track Roadway is mainly located in the front and upper part, and the gas source is mainly 5# coal seam under the roadway; The range of surrounding rock loose circle formed after roadway excavation is 0.65 ~ 2.30 m.

3) In alignment with the specific conditions of the 221 East Wing Track Roadway, which is situated between coal seams, the high and low negative pressure dual drainage interception technology is employed to effectively intercept gas primarily originating from the 5# coal seam beneath the roadway. This approach significantly contributes to ensuring the safe excavation of the roadway.

6. Statements

6.1 Funding

Not Applicable.

6.2 Competing Interests

The authors have no relevant financial or non-financial interests to disclose.

6.3 Author Contributions

Fake Ren and Chongyang Wang were responsible for report analysis and paper writing. Jie Li and Weiwei Su helped in writing the paper.

6.4 Data Availability

The datasets generated during and analyzed during the current study are available from the corresponding author on reasonable request.

References

[1] Peng J, Leng Y, Zhu X, et al. Development of a loess-mudstone landslide in a fault fracture zone. Environ Earth Sci. 2016; 75:658. https://doi.org/10.1007/s12665-016-5336-8.

[2] Cheng H,.Chen J, Chen G. Analysis of ground surface settlement induced by a large EPB shield tunnelling: A case study in Beijing, China. Environ. Earth. Sci. 2019; 78:605. https://doi.org/10.1007/s12665-019-8620-6.

[3] Yoshida H, Nagatomo A, Oshima A, et al. Geological characterization of the active Atera Fault in central Japan: implications for defining fault exclusion criteria in crystalline rocks around radioactive waste repositories. Eng Geol 2014; 17:93-103. https://doi.org/10.1016/j.enggeo.2014.05.008.

[4] Zimmerman R, Al-Yaarubi A, Pain C, et al. Non-linear regimes of fluid flow in rock fractures. Int J Rock Mech Min Sci 2004; 41:384. https://doi.org/10.1016/j.ijrmms.2003.12.045.

[5] Al-Rbeawi S. New technique for determining rate dependent skin factor & non-Darcy coefficient. J Nat Gas Sci Eng 2016; 35:1044-1058. https://doi.org/10.1016/j.jngse.2016.09.028.

[6] Liu W, Zhou Y, Chu X, et al. Effects of seepage behaviors on coal spontaneous combustion in longwall gobs: an investigation between Darcy and non-Darcy seepage. Fuel 2022; 322:124126. https://doi.org/10.1016/j.fuel.2022.124126.

[7] Yang T, Jia P, Shi W, et al. Seepage–stress coupled analysis on anisotropic characteristics of the fractured rock mass around roadway. Tunn Undergr Sp Tech 2014; 43:11-19. http://dx.doi.org/10.1016/j.tust.2014.03.005.

[8] Zhu B, Song Y, Wu B, et al. Experimental study on the effects of vibrational frequency on the permeability of gas-containing coal rocks. Arch Min Sci 2021; 66:265-278. https://doi.org/10.24425/ams.2021.137461.

[9] Yan M, Yang F, Zhang B, et al. Influence of pore structure characteristics of low permeability coal on Gas Nonlinear Seepage. Nat Resour Res, 2024; 33:1209-1225. https://doi.org/10.1007/s11053-024-10325-5

588 [10] Liu J, Gao J, Zhang X, et al. Experimental study of the seepage characteristics of loaded coal under
589 true triaxial conditions. Rock Mech Rock Eng 2019; 52:2815–2833. https://doi.org/10.1007/s00603-
590 018-1720-x.
591 [11] Zhou F, Xia T, Wang X, et al. Recent developments in coal mine methane drainage and utilization in
592 China: A review. J Nat Gas Sci Eng 2016; 31:437-458. http://dx.doi.org/10.1016/j.jngse. 2016.03.027.
593 [12] Zhu X, Wei S, Luo W, et al. Numerical simulation and experimental study on improving gas drainage
594 by hydraulic fracturing. Energy Sources 2023; 45(1):1965-1982. https://doi.org/10.1080/15567036.
595 2023.2182849.
596 [13] Zhang R, Wang P, Cheng Y. A new technology to enhance gas drainage in the composite coal seam
597 with tectonic coal sublayer. J Nat Gas Sci Eng 2022; 106:104760. https://doi.org/10.1016/j.jngse.
598 2022.104760.
599 [14] Niu X, Pang D, Liu H, et al. gas drainage mechanism and effect of ultra-high-pressure hydraulic
600 slotting technology: a case study in renlou coal mine. Nat Resour Res 2023; 32(1):321-339.
601 [15] Linghu J, Chen H, Wang L. New technology of mechanical cavitation in a coal seam to promote gas
602 drainage. ACS Omega 202 2; 7:21163-21171. https://doi.org/10.1021/acsomega.2c01962.
603 [16] Xu W, Zheng X, Liu C, et al. Numerical simulation study of high-pressure air injection to promote
604 gas drainage. Sustainability 2022; 14:13699. https://doi.org/10.3390/su142113699.
605 [17] Wang H, Cheng Z, Zou Q, et al. Elimination of coal and gas outburst risk of an outburst-prone coal
606 seam using controllable liquid CO2 phase transition fracturing. Fuel 2021; 284: 119091.
607 https://doi.org/10.1016/j.fuel.2020.119091.
608 [18] Qi R, Qin X, Lu C, et al. Experimental study on the isothermal adsorption of methane gas in natural
609 gas hydrate argillaceous silt reservoir. Adv Geo-Energy Res 2022; 6(2):143-156. https://doi.

610 org/10.46690/ager.2022.02.06.

611 [19] Li H, Ma J, Wang Z, et al. A gas outburst prevention and control strategy for single thick coal seams
612 with high outburst risk: A case study of Hudi Coal Mine in Qinshui Basin. Energy Sci Eng 2020;
613 8:2471-2491. https://doi.org/10.1002/ese3.680.

614 [20] Szlązak N, Obracaj D, Swolkień J. Methane drainage from roof strata using an overlying drainage
615 gallery. Int J Coal Geol 2014; 136: 99-115. http://dx.doi.org/10.1016/j.coal.2014.10.009

616 [21] Zheng C, Jiang B, Xue S, et al. Coalbed methane emissions and drainage methods in underground
617 mining for mining safety and environmental benefits: A review. Process Saf Environ 2019; 127:103-
618 124. https://doi.org/10.1016/j.psep.2019.05.010

619 [22] Hosseini A, Najafi M. Determination of methane desorption zone for the design of a drainage
620 borehole pattern (case study: e4 panelof the tabas mechanized coal mine,Iran). Rud-Geol-Naft Zb,
621 2021; 36: 61-75. https:/doi.org/10.17794/rgn.2021.1.6

622 [23] Liu B, Liu Z, Li S, et al. Comprehensive surface geophysical investigation of karst caves ahead of
623 the tunnel face: A case study in the Xiaoheyan section of the water supply project from Songhua
624 River, Jilin, China. J Appl Geophys 2017; 144:37-49. https://doi.org/10.1016/j.jappgeo.2017.06.013.

625 [24] Xue G, Chen W, Cheng J, et al. A review of electrical and electromagnetic methods for coal mine
626 exploration in china. Ieee Access 2019; 7:177332-177341. https://doi.org/10.1109/ACCESS.2019.
627 2951774.

628 [25] Liu M, Liu Z, Zhou D, et al. Recognition method of typical anomalies during karst tunnel
629 construction using GPR attributes and Gaussian processes. Arab J Geosci 2020; 13:791. https://doi.
630 org/10.1007/s12517-020-05782-0.

631 [26] Wang Z, Sheng J, Wang R, et al. Analysis of Microtremor Exploration Application and Construction

632 Monitoring in a Large-Diameter Shield Tunnel. Appl Sci-Basel 2023; 13:263. https://doi.org/10.
633 3390/app13010263.
634 [27] Guo L, Chen J, Cui X, et al. Application of ground penetrating radar for coarse root detection and
635 quantification: a review. Plant Soil 2013; 362:1-23. https://doi.org/10.1007/s11104-012-1455-5.
636 [28] Ma Y, Fan X, Mo W, et al. Catalytic hydrogenation and heteroatom removal for isopropanol soluble
637 organic matter of Dongming lignite. Fuel Process Technol 2021; 211:106589. https://doi.org/10.
638 1016/j.fuproc.2020.106589.
639 [29] Zou C, Tao S, Han W, et al. Geological and geochemical characteristics and exploration prospect of
640 coal-derived tight sandstone gas in china: case study of the ordos, sichuan, and tarim basins. Acta
641 Geologica Sinica (English Edition) 2018; 92(4):1609-1626. https://doi.org/10.1111/1755-6724.
642 13647.
643 [30] Guo X, Zhao Z, Gao X, et al. Analytical solutions for characteristic radii of circular roadway
644 surrounding rock plastic zone and their application. Int J Min Sci Techno 2019; 29:263-272.
645 https://doi.org/10.1016/j.ijmst.2018.10.002.
646 [31] Kang H, Gao F, Xu G, et al. Mechanical behaviors of coal measures and ground control technologies
647 for China’s deep coal mines - A review. J Rock Mech Geotech 2023; 15:37-65. https://doi.
648 org/10.1016/j.jrmge.2022.11.004.
649 [32] Wang X. Evaluation of underground hydraulic fracturing using transient electromagnetic method.
650 Environ Sci Pollut R 2019; 26: 1458-11469. https://doi.org/10.1007/s11356-019-04539-x
651 [33] Wang R, Deng H, Meng Y, et al. Case study of modified h-b strength criterion in discrimination of
652 surrounding rock loose circle. Ksce J Civ Eng 2019; 23(3):1395-1406. https://doi.org/10.
653 1007/s12205-019-1055-5 .

[34] Li F, Jin L, Han H, et al. Structural analysis and study on support technology of refuge chamber of mine. Applied Mechanics and Materials 2012; 204-208: 1356-1361. https://doi.org/10.4028/www.scientific.net/AMM.204-208.1356

[35] Chu H, Li G, Liu Z, et al. Multi-level support technology and application of deep roadway surrounding rock in the suncun coal mine, china. Materials 2022; 15:8665. https://doi.org/10.3390/ma15238665.

[36] Yang S, Hua X, Liu X, et al. Analysis of stability factors of roadway roof and determination of unsupported roof distance. Shock Vib 2021; 2271257. https://doi.org/10.1155/2021/2271257.

[37] Ajit, Iqbal Ahmed Khan. Experimental work on the low Reynolds number behaviour of 2-hole offset probes. International Journal of Engineering and Advanced Technology (IJEAT) 2020; 449-454. https://doi.org/10.35940/ijeat.e9669.069520

[38] Liu Z, Hu P, Yang H, et al. Coupling mechanism of coal body stress–seepage around a water injection borehole. Sustainability 2022; 14:9599. https://doi.org/10.3390/su14159599.

[39] Liu Q, Cheng Y, Zhou H, et al. A mathematical model of coupled gas flow and coal deformation with gas diffusion and klinkenberg effects. Rock Mech Rock Eng 2015; 48:1163-1180. https://doi.org/10.1007/s00603-014-0594-9.